Extreme rainfall activity in the Australian tropics reflects changes in the El Niño/Southern Oscillation over the last two millennia

Rhawn F. Denniston[a,1], Gabriele Villarini[b], Angelique N. Gonzales[a], Karl-Heinz Wyrwoll[c], Victor J. Polyak[d], Caroline C. Ummenhofer[e], Matthew S. Lachniet[f], Alan D. Wanamaker, Jr[g], William F. Humphreys[h], David Woods[i], and John Cugley[j]

[a] Department of Geology, Cornell College, Mount Vernon, IA 52314

[b] IIHR-Hydroscience & Engineering, University of Iowa, Iowa City, IA 52240

[c] School of Earth and Environment, 35 Stirling Highway, University of Western Australia, Crawley, Western Australia 6009

[d] Department of Earth and Planetary Sciences, University of New Mexico, Albuquerque, NM 87131

[e] Department of Physical Oceanography, Woods Hole Oceanographic Institution, Woods Hole, MA 02543

[f] Department of Geoscience, University of Nevada Las Vegas, Las Vegas, NV 89154

[g] Department of Geological and Atmospheric Sciences, Iowa State University, Ames, IA 50011

[h] Western Australia Museum, Locked Bag 49, Welshpool DC, Western Australia 6986

[i] Department of Parks and Wildlife, PO Box 65, Broome, Western Australia 6725

[j] Australian Speleological Federation, Willetton, Western Australia 6155

rdenniston@cornellcollege.edu; tel: 319-895-4306

Classification: Physical Science (Earth, Atmospheric, and Planetary Sciences)

Keywords: speleothem, tropical cyclone, monsoon, El Niño/Southern Oscillation, Australia

Abstract

Assessing temporal variability in extreme rainfall events prior to the historical era is complicated by the sparsity of long-term 'direct' storm proxies. Here we present a 2200-yr-long, accurate and precisely dated record of cave flooding events from the northwest Australian tropics that we interpret, based on an integrated analysis of meteorological data and sediment layers within stalagmites, as representing a proxy for extreme rainfall events derived primarily from tropical cyclones (TCs) and secondarily from the regional summer monsoon. This time series reveals substantial multi-centennial variability in extreme rainfall, with elevated occurrence rates characterizing the twentieth century, the period 850-1450 CE, and 50-400 CE; reduced activity marks 1450-1650 CE and 500-850 CE. These trends are similar to reconstructed numbers of TCs in the North Atlantic and Caribbean basins, and form temporal and spatial patterns best explained by secular changes in the dominant mode of the El Niño-Southern Oscillation (ENSO), the primary driver of modern TC variability. We thus attribute long-term shifts in cyclogenesis in both the central Australian and North Atlantic sectors over the past two millennia to entrenched El Niño or La Niña states of the tropical Pacific. The influence of ENSO on monsoon precipitation in this region of northwest Australia is muted, but ENSO-driven changes to the monsoon may have complemented changes to TC activity.

Significance Statement

Variations in TC activity are poorly known prior to the twentieth century, complicating our ability to understand how cyclogenesis responds to different climate states. We used stalagmites to develop a near-annual record of cave flooding from the central Australian tropics where TCs are

responsible for the majority of extreme rainfall events. Our 2200-year time series reveals shifts in the mean number of storms through time, similar to TC variability from the North Atlantic. This finding is consistent with modern relationships between ENSO and cyclogenesis, as well as with the reconstructed state of ENSO over the past two millennia, suggesting that changes between La Niña- and El Niño-dominated periods drove multi-centennial shifts in TC activity in both basins.

/body

Introduction

Two primary components of tropical precipitation - monsoons and TCs – are capable of producing high volumes of rainfall in short periods of time (extreme rainfall events) that lead to flooding. Because both systems respond to changes in atmospheric and sea surface conditions (1, 2), it is imperative that we understand their sensitivities to climate change. For example, over recent decades, warming of the oceans has driven increases in the mean latitude (3) and energy released by TCs (4). These storms (a.k.a. hurricanes, typhoons, tropical storms, and tropical depressions) can produce enormous economic and societal disruptions but also represent important components of low latitude hydroclimate (5) and ocean heat budgets (6). Monsoon reconstructions spanning the last several millennia have been developed using a variety of proxies (7-10), including stalagmites (11-13), but reconstructing past TC activity is generally more difficult. In most of the world's ocean basins, accurate counts of TCs are limited to the start of the satellite era (since 1970 CE), an interval too short to capture changes occurring over multi-decadal to centennial time scales. Therefore, as a complement to the historical record, sedimentological analyses of storm-sensitive sites have formed the basis of TC reconstructions, primarily in and around the North Atlantic and Caribbean basins (14-19) that largely focus on near-coastal sequences, including beach ridges,

overwash deposits, and shallow marine sediments. Together, these studies have revealed that North Atlantic and Caribbean TC activity varied substantially over the past several centuries to millennia, with multi-centennial shifts attributed to a range of factors including atmospheric dynamics in the North Atlantic, North African rainfall, and ENSO.

Today, ENSO represents a dominant control of inter-annual TC activity at a global scale through its influences on surface ocean temperature gradients and atmospheric circulation (20-23). However, no record has clearly demonstrated the link between ENSO and prehistoric TCs in the tropical Pacific, Indian, or Australian regions, leaving unanswered questions about the sensitivity of cyclogenesis to ENSO prior to the modern era. This issue is of particular concern given modeling results that predict changes in ENSO behavior may accompany anthropogenic warming of the atmosphere (24, 25). Fully assessing the sensitivity of TCs to changes in climate requires high-resolution and precisely dated paleostorm reconstructions from multiple basins spanning periods beyond those available in observational data, a goal that has largely proven elusive. Few such records unambiguously derived from TCs have been identified, particularly in the western Pacific and Indo-Pacific (20, 26-30).

Study Area and Conceptual Model

We present a near annual resolution flood record from cave KNI-51 in the central Australian tropics (Fig. 1), an area that experiences intense TC- and monsoon-derived rainfall. KNI-51 (15.18˚S, 128.37˚E, ~100 m elevation) is located in the low-lying Ningbing range of the eastern Kimberley of tropical Western Australia, ~20 km south of the Timor Sea (Fig. 1). The cave consists largely of a single horizontal passage, 600 m in length and accessed by a $2m^2$ entrance located along the valley floor. Clear evidence of flooding is apparent in KNI-51 and includes mud staining on

cave walls and speleothems (Fig. 2). Extreme rainfall events flood the cave, suspending fine-grained sediment that coats stalagmite surfaces. Mud layers are encapsulated within these rapidly growing stalagmites after floodwaters recede and growth resumes (31) (Fig. 2). The ages of flood layers, which range in thickness from <1-10 mm, are tightly bracketed by precise ^{230}Th dating (typically within ± 20 yr; 2 standard deviations) of the stalagmite aragonite. The KNI-51 flood record spans the majority of the last 2200 yr, thereby allowing an examination of the nature of extreme rainfall events across a time span well beyond the reach of direct observation.

The seven stalagmites analyzed in this study were collected from the base of the inclined mud embankment on which they had grown, ~500 m from the entrance; the majority of stalagmites were broken and down when collected (SI Appendix, Fig. S1). To calibrate the flood signal, 16 ^{230}Th dates with errors of ±1-2 yr were used to determine the ages of mud layers deposited between the years 1908 – 2009 CE in the actively growing sample (KNI-51-11) (Materials and Methods; SI Appendix, Fig. S2 and Table S1). Growth was continuous over the last century but a change in drip position from the center to the margin of the stalagmite in ~1986 CE produced an inclined growth surface that made mud preservation less reliable after this time (Materials and Methods; SI Appendix, Fig. S3). An additional 33 dates constrain the ages of the six older stalagmites (13), with errors on all stalagmites averaging ±30 yr .

The hydroclimate of the Kimberley is dominated by TCs and the Indo-Australian Summer Monsoon (IASM), both of which occur predominantly during austral summer/early fall (December – March) in association with the development of the IASM trough (32). As a result, the region experiences substantial seasonal variability in rainfall, with mean annual precipitation exceeding 800 mm (SI Appendix, Fig. S4). Summer rainfall variability is linked to a number of factors including ENSO (32-35). But while there is an appeal in the paleoclimate literature for ENSO to

have exerted a significant impact on summer precipitation throughout the Australian tropics (13, 36), the impact of ENSO on the monsoon rainfall regime of northwestern Australia is complex. Canonical ENSO events typically have a muted impact on IASM rainfall in this region (33, 37) with La Niña (El Niño) events resulting in only mildly wetter (drier) monsoon seasons. The recently recognized El Niño Modoki may be the exception, with such events seemingly characterized by a shortened monsoon season containing above average rainfall in some months (38). Rainfall from both TCs and the IASM can be intense, with one-day totals capable of exceeding 160 mm and maximum three-day totals approaching 500 mm near KNI-51.

We constrained the precipitation threshold required to flood KNI-51 by comparing daily rainfall data from Carlton Hill Station, the most proximal weather station to the cave site (~40 km), with mud layers in stalagmite KNI-51-11. Carlton Hill Station offers a discontinuous record of daily rainfall data, with the longest gap spanning 1977-1982 CE. Maximum three-day rainfall accumulations provided the strongest relationship between flood occurrence and rainfall (p-value < 0.015; SI Appendix, Fig. S5 and S6) and therefore represent the most likely mechanism for triggering cave flooding. To assess the strength of the link between TCs and precipitation, we examined which of the maximum three-day rainfall events could be associated with the passage of a TC within a 600-km radius, a window size selected to capture TC rainfall effects (5, 39) (Materials and Methods; SI Appendix, Fig. S7). Approximately two-thirds of extreme rainfall events exceeding 200 mm were related to TCs, while all of the events in excess of 250 mm were TC-related (Fig. 3). TCs are similarly responsible for the vast majority of the heaviest 1- and 2-day rainfall events. These numbers are striking considering that observational capabilities were limited prior to 1970 CE (and thus some TCs likely were not properly identified), and support the notion that TCs are responsible for the majority of heavy rainfall events, and thus flooding, at KNI-51 (Fig.

3). The veracity of the relationship is further supported by similar changes in TC occurrences and cave flood frequencies between 1908-1986 CE (SI Appendix, Fig. S8), although non-stationarity of this relationship may be expected in prehistorical periods.

As a test of the influence of multi-decadal changes in the IASM on our record, we compared our flood time series with oxygen isotope variations within the same stalagmites. Oxygen isotopic ratios in monsoon-derived rainwater are largely controlled by the intensity of precipitation events (the so-called "amount effect") (40), and rainwater derived from TCs can also be anomalously depleted in ^{18}O (41). Infiltrating water from both systems may be preserved within stalagmite carbonate, thereby tracking the strength of the paleomonsoon (13) and, in some cases, past TC activity (26, 29, 42) although extremely high temporal resolution and precise age control are required. Little consistent correspondence is observed between flood events and stalagmite oxygen isotope values, as would be expected if heavy rainfall was simultaneously controlling both oxygen isotope variations and flooding events (SI Appendix, Fig. S9). This observation demonstrates that the oxygen isotopic ratios of TC rainfall are poorly coupled to TC frequency at KNI-51, likely due to the fact that infiltration rate into KNI-51 is rapid, and that stalagmites are routinely submerged (and thus not precipitating aragonite) during extreme rainfall events (SI Appendix).

The KNI-51 flood record marks the first precisely dated, high-resolution extreme rainfall reconstruction for the central Australian tropics and Indo-Pacific and shows pronounced multi-centennial-scale variability. Our record – which based on these meteorological analyses and monsoon reconstruction we interpret as largely reflecting TC activity – reveals moderate numbers of extreme rainfall events during 850-1450 and 1800-2000 CE, and low numbers of extreme rainfall events from 500-850 and 1450-1650 CE (no stalagmite was identified that spanned 1650-1750 CE) (Fig. 4). A sharp spike in cave flooding activity at ~1890 CE occurs synchronously with the

introduction of cattle grazing to the area surrounding KNI-51 and that likely triggered a temporary change in surface hydrology which may have biased the historical portion of this record (Fig. 4; SI Appendix). The shortest recurrence rates (the highest extreme rainfall activity) and also the greatest variability occurred from 50-400 CE, with peak values three times those of the 16th century.

Drivers of Tropical Cyclone Variability

Today, ENSO is recognized as one of the primary drivers of global TC variability, and ENSO impacts the Australian and North Atlantic (including the Caribbean) regions similarly (22, 23). During La Niña years in the instrumental record, both north Australian and North Atlantic TCs are 20% more likely to occur than in El Niño years (21, 43) because cool eastern Pacific SST and steeper zonal Pacific SST gradients during La Niña events enhance low-level atmospheric vorticity in the Atlantic and Australian main development regions while decreasing vertical shear of zonal winds (22, 23, 43) (Fig. 1).

Several studies have examined ENSO as a driver of past TC variability (16, 18-20, 30), but a primary obstacle to understanding the influence of ENSO on prehistoric TCs is the fact that the dynamical nature of ENSO over the late Holocene remains controversial, with no clear consensus yet reached on the timing or sign of ENSO prior to instrumental records (44-52). Our data provide strong support for the hypothesis that the medieval period (9th-15th centuries) was characterized by an enhanced La Niña-like climate state in the tropical Pacific Ocean, as has been suggested by numerous previous studies (44, 45, 47-49), explaining the observed elevated TC activity during this time; more El Niño-like conditions characterized much of the 16th-19th centuries, consistent with the reduced TC activity after 1450 CE (Fig. 4).

These trends in Australian TC activity are strikingly similar to those from multiple sites across the North Atlantic and Caribbean basins. Recent reconstructions of Gulf of Mexico (14) and Caribbean (15) hurricanes revealed peak activity during medieval times followed by a sharp decline into the 16th-19th centuries (Fig. 4). And a synthesis of TC reconstructions based on eight sites from Puerto Rico and the East Coast of the United States for the last 1500 years also identified elevated numbers of storms during this time, although significant intra-site variability exists (16) (Fig. 4). Such synchronous shifts between more and less active TC regimes in the Australian and North Atlantic regions agree with modern ENSO teleconnections and are consistent with marine studies from ENSO-sensitive areas of the Peruvian margin in the eastern Pacific (44) and the Makassar Straight of the Indo-Pacific (52) that show enhanced La Niña activity during medieval times relative to periods subsequent or prior. A prominent feature of the KNI-51 time series (present in two of three stalagmites that span this interval) is a peak in TC activity at 1350 CE (SI Appendix, Fig. S12). Peak numbers of La Niña events are indicated in both the eastern Pacific and Indo-Pacific at this time (Fig. 4), suggesting a causal link although other influences on Australian TC activity also exist, including the Madden Julian Oscillation (53, 54) and extra-tropical phenomena such as the Southern Hemisphere Annular Mode (SAM), a mid- to high-latitude dipole of tropospheric atmospheric pressure. Reconstructions of the SAM reveal a short-lived shift around 1300-1350 CE that could help account for some of the storms in the 14th century (55). The highest storm activity of the entire 2200 yr record occurs as three ~50 yr-long peaks centered on 100, 200, and 350 CE. A similar pattern was also reconstructed from a Belize marine sequence (15) (highest hurricane activity of past 1500 yr at 200 CE), and from a northeastern Mexico stalagmite (31) (highest hurricane activity of the past 2000 yr between 50 – 350 CE). In addition, a 5000-yr hurricane reconstruction from Puerto Rico sediments records the highest prehistorical TC activity of the last

two millennia as three sharp peaks between 0-500 CE, nearly identical in timing to the KNI-51 record (although the Puerto Rico time series lacks multi-centennial shifts associated with the medieval and 16th-19th century intervals) (19) (Fig. 4). However, neither of the high-resolution ENSO reconstructions from the eastern Pacific or Indo-Pacific record enhanced numbers of La Niña events at this time. Thus, addressing this question requires extending accurate, high-resolution ENSO reconstructions from the Pacific basin through the past several millennia.

The influence of ENSO on TC genesis is similar across much of (sub)tropical Australia, including from the western (Cape Range) and northeastern (Chillagoe) portions of the continent (Fig. 1), the sites of recently developed TC reconstructions based on oxygen isotopic ratios in stalagmites (26, 29). The KNI-51 time series differs sharply from these records, with no multi-centennial TC variability coincident with either the medieval or 16th-19th century periods at Cape Range, and *elevated* TC activity during the 16th-19th centuries in the Chillagoe time series. Today, ENSO impacts cyclogenesis at these sites similarly to the Kimberley (23), and thus the differences between them may reflect climatological origins such as drivers other than ENSO on TC formation or steering (23), rainfall derived from sources other than TCs (i.e., the IASM at KNI-51 and northwest cloud bands at Cape Range[56]), or phenomena such as so-called "masking effects" (57) or kinetic influences on oxygen isotopic values (58) – signals that can be difficult to detect in individual stalagmites; these are important questions that should be addressed in future studies.

Attribution of Australian and Atlantic TC variability to ENSO over the last two millennia serves to re-focus attention on the links between a warming world and the tropical Pacific Ocean. Most (22, 59), but not all (2) down-scaled computer models suggest that a decrease in global numbers of TCs will accompany future warming. However, increased greenhouse gas concentrations are likely to shift the heat budget of the western Pacific, which could favor enhanced

cyclogenesis if not counteracted by a dynamical response to more El Niño-like conditions. Should the Pacific Ocean transition to a more El Niño-like climate state, as suggested by some model results (24), then less frequent TCs may become the norm over coming decades to centuries. ENSO modulation of extreme rainfall events – largely through TCs but also through less pronounced impacts on the IASM – should be considered in hydroclimate models of the Indo-Pacific.

Materials and Methods

Flood Layer Analysis. Each KNI-51 stalagmite was bisected along its vertical growth axis using a water-cooled rock saw. Accumulations of mud layers, ranging in height from <1 to 10 mm, drape numerous growth horizons throughout each sample. The position of flood layers was measured to the nearest half-mm from the base of the stalagmite and fitted to the growth model derived from the ^{230}Th dates. This growth model was adjusted to account only for the deposition of stalagmite carbonate and is not distorted by the thickness of individual mud layers. Preservation and detection of flood-derived mud layers in stalagmites is subject to several caveats. First, as they grow, stalagmites require increasingly deep floodwaters to deposit mud on their caps. Secondly, mud deposits form a zone of structural weakness within a stalagmite that could be eroded by later floods, erasing evidence of previous storm events. Third, the geometry of individual stalagmites impacts their ability to preserve mud layers. Angular tops on thin stalagmites or steeply inclined tops form the least suitable geometries to preserve sediment deposited by flooding. In many cases, mud layers were most visible on the cap margins suggesting that some sediment was eroded by dripwater prior to crystallization of aragonite. Because of this fact, the position in which each stalagmite was bisected introduced some degree of variability into our ability to recognize and classify mud layers. The majority of stalagmites were broken and down when collected at the base of the mud bank on

which they grew, 1-2 m below recent flood markers preserved on the cave walls. We attempted to address these potential problems by using stalagmites formed below the height of cave flood markers, by obtaining a high number of precise radiometric dates, particularly during the twentieth century, the period of calibration, and wherever possible, by constructing time series from multiple, coeval stalagmites.

Mud layers were assigned to one of four categories depending on the maximum defined thickness of mud accumulation: Type 1: < 0.5 mm; Type 2: 0.5-1.0 mm; Type 3: > 1.0 mm (SI Appendix, Fig. S10). Numerous stains on stalagmite growth surfaces are also present (designated as Type 0) but since no appreciable mud accumulation is apparent in these layers, they can not be interpreted unambiguously as resulting from cave flooding events and thus were not included in our record. However, including Type 0 events in the time series resulted in an increase in the frequency of cave flooding events but largely maintained the overall patterns (SI Appendix, Fig. S11). The distribution of these types varied between stalagmites, in part because differentiation between flood types is to some degree subjective and includes the biases associated with preservation. Sample KNI-51-10 is somewhat unusual in that it is characterized exclusively by Type 1 (and Type 0) events. The fine-scale interlayering of flood layers in this sample are responsible for the markedly lower precision on its ^{230}Th dates relative to the other stalagmites.

Identifying biases within individual stalagmites marks an important step in assessing their utility as paleostorm indicators (31). The flood records from coeval stalagmites reveal similar variability at multi-decadal scales; the only exception is KNI-51-G (1340-1640 CE) that records flood occurrence rates marginally higher than those observed in the two other stalagmites of similar age although short-term and long-term trends in flood activity are nearly identical (SI Appendix, Fig. S12). The origin of this discrepancy is unclear but may be related to biases associated with

flood layer preservation or identification, or the elevation at which this stalagmite grew on the mud bank.

^{230}Th Dating. Samples for dating were milled by a hand-held Dremel tool or by using a computer-guided drill with either a 1 or 2 mm-diameter bit. Radioisotopic ages were obtained with ^{238}U-^{234}U-^{230}Th disequilibrium techniques at the University of New Mexico, and ages of mud layers were determined by polynomials fit to dated intervals. Approximately 50-100 mg of aragonite was milled from each interval of interest and then dissolved, spiked with a mixed ^{229}Th-^{233}-U-^{236}U tracer, and processed using column chemistry methods. The U and Th fractions were dissolved in a 3% HNO_3 4 ml solution which was then aspirated into a Thermo Neptune MC-ICP-MS using a Cetac Aridus II low flow (50–100 µl/min) desolvating nebulizer system. U and Th separates were run as static routines where all isotopes were measured in Faraday cups, with the exception of ^{230}Th, which was measured using the secondary electron multiplier (SEM). Gains between the SEM and Faraday cups were determined using standard solutions of NBL-112 for U and an in-house ^{230}Th-^{229}Th standard for Th, both of which were measured routinely. U and Th blanks are <20 pg and half-lives of ^{230}Th and ^{234}U are those of ref. 60. Unsupported ^{230}Th was corrected for using an initial ^{230}Th/^{232}Th ratio equal to the average crustal silicate value of 4.4×10^{-6} (±50%). Because ^{232}Th concentrations were very low, the ages of the uncorrected and detritral Th-corrected ages were nearly identical. Elevated U abundances and δ^{234}U values, low detrital Th (^{232}Th) concentrations, and high growth rates allowed extremely precise age determinations on samples as young as one year old (Table S1).

Calibrating the KNI-51 flood record. Considering only those years containing complete wet season rainfall data (December-March), the stalagmite and rainfall time series overlapped for a total of 66 years between 1908-2008 CE. We calculated one-, two-, and three-day maximum rainfall totals over the December-March period, and compared these data to the KNI-51-11 flood layer time series. Flood events were assigned to individual years, and a best-case correspondence was calculated by shifting the mud layer ages by up to ±1 yr (the minimum age model uncertainties) to maximize their fit to these peak rainfall events, thereby preserving the temporal continuity of the mud layers. This is a somewhat conservative method given that it does not allow for compression or expansion of ages for consecutive flood layer events, even if it was possible within the errors of the dates to do so while still maintaining stratigraphic superposition. Because of the binary nature of the data (occurrence or non-occurrence of a flood event), we used logistic regression to examine the relationship between extreme rainfall and flood events. Our expectation is that the larger the rainfall amount, the higher the probability of flooding (Fig. S6).

ACKNOWLEDGMENTS. This manuscript benefited greatly from comments by editor Kerry Emanuel and three anonymous reviewers. Funding was provided by the Paleo Perspectives on Climate Change (P2C2) program of the United States National Science Foundation (NSF) through grant AGS-1103413, a seed grant from the Center for Global and Regional Environmental Research, and Cornell College (all to R.D.), the Kimberley Foundation Australia (to K-H.W.), and Penzance and John P. Chase Memorial Endowed Funds at WHOI (to C.U.). We thank Donna Cavlovic for assistance at KNI-51 and in Kununurra. Yemane Asmerom and the Radiogenic Isotope Laboratory at the University of New Mexico supported much of the chronology work through NSF ATM-0703353 (to Y.A. and V.J.P.), and EAR-0326902 (to Y.A. and others).

Author Contributions. R.D. and K-H.W. designed the study; R.D., J.C., D.W., and W.H. conducted the fieldwork; R.D., V.P., and A.G. performed the dating; A.G. and R.D. obtained the flood layer measurements; G.V. conducted the rainfall/flood layer statistical analysis and developed most figures except for Fig. 1 which was constructed by C.U.; R.D. wrote the manuscript with contributions from G.V., V.P., A.G., A.W., M.L., K-H.W., C.U., and W.H.; all authors contributed to finalizing and approving the manuscript.

References

1. Li X-F, Yu J, Li Y (2013) Recent summer rainfall increase and surface cooling over Northern Australia since the late 1970s: a response to warming in the Tropical Western Pacific. *J Clim* 26: 7221–7239.
2. Emanuel K (2013) Downscaling CMIP5 climate models shows increased tropical cyclone activity over the 21st century. *Proc Nat Acad Sci* 110: 12219-12224.
3. Kossin J, Emanuel K, Vecchi G (2014) The poleward migration of the location of tropical cyclone maximum intensity. *Nature* 509: 349-352.
4. Emanuel K (2005) Increasing destructiveness of tropical cyclones over the past 30 years. *Nature* 436: 686-688.
5. Dare R, Davidson N, McBride J (2012) Tropical cyclone contribution to rainfall over Australia. *Mon Weath Rev* 140: 3606-3619.
6. Mei W, Primeau F, McWilliams J, Pasquero C (2013) Sea surface height evidence for long-term warming effects of tropical cyclone on the ocean. *Proc Nat Acad Sci*, www.pnas.org/cgi/doi/10.1073/pnas.1306753110.
7. Wyrwoll K-H, Miller G (2001) Initiation of the Australian summer monsoon 14,000 years ago. *Quat Int* 83-85: 119-128.
8. Russell, J and Johnson T (2007) Little Ice Age drought in equatorial Africa: intertropical convergence zone migrations and El Niño-Southern Oscillation variability. *Geology* 35: 21-24.
9. Tierney J, Oppo D, Rosenthal Y, Russell J, Linsley B (2010) Coordinated hydrological regimes

in the Indo-Pacific region during the past two millennia. *Paleocean* 25: PA1102.

10. Mohtadi M *et al*. (2011) Glacial to Holocene swings of the Australian-Indonesian monsoon. *Nat Geo* 4: 540-544.
11. Zhang P *et al*. (2008) A test of climate, sun, and culture relationships from an 1810-year Chinese cave record. *Science* 322: 940-942.
12. Griffiths M *et al*. (2009) Increasing Australian-Indonesian monsoon rainfall linked to early Holocene sea-level rise. *Nat Geo* 2: 636-639.
13. Denniston R *et al*. (2013) A Stalagmite Record of Holocene Indonesian-Australian Summer Monsoon Variability from the Australian Tropics. *Quat Sci Rev* 78: 155-168; 10.1016/j.quascirev.2013.08.004.
14. Lane P, Donnelly J, Woodruff J, Hawkes, A (2011) A decadally-resolved paleohurricane record archived in the late Holocene sediments of a Florida sinkhole. *Mar Geo* 287: 14-30.
15. Denommee K, Bentley S, Droxler A (2014) Climatic controls on hurricane patterns: a 1200-y near-annual record from Lighthouse Reef, Belize. *Sci Rep* 4: 1-7.
16. Mann M, Woodruff J, Donnelly J, Zhang Z (2009) Atlantic hurricanes and climate over the past 1,500 years. *Nature* 460: 880-883.
17. Scileppi E, Donnelly J (2007) Sedimentary Evidence of Hurricane Strikes in Western Long Island, New York. *Geochem Geophy Geosys* 8: Q06011; doi:10.1029/2006GC001463.
18. Donnelly J, Woodruff J (2007) Intense hurricane activity over the past 5,000 years controlled by El Niño and the West African monsoon. *Nature* 447: 465-468.
19. Woodruff J, Donnelly J, Mohrig D, Geyer W (2008) Reconstructing relative flooding intensities responsible for hurricane-induced deposits from Laguna Playa Grande, Vieques, Puerto Rico. *Geology* 36: 391-394.
20. Nott J, Forsythe A (2012) Punctuated global tropical cyclone activity over the past 5,000 years. *Geophys Res Lett* 39: L14703.
21. Kuleshov Y (2012) Southern Hemisphere Tropical Cyclone Climatology, Modern Climatology, Dr Shih-Yu Wang (Ed.), InTech, http://www.intechopen.com/books/modern-climatology/southern-hemisphere-tropical-cyclone-climatology.
22. Camargo S, Emanuel K, Sobel A (2007) Use of a Genesis Potential Index to diagnose ENSO effects on tropical cyclone genesis. *J Clim* 20: 4819-4834.
23. Ramsay H, Camargo S, Kim D (2012) Cluster analysis of tropical cyclone tracks in the Southern

Hemisphere. *Clim Dyn* 39: 897-917.

24. Vecchi G, Soden B (2007) Global warming and the weakening of the tropical circulation. *J Clim* 20: 4316-4340.
25. Collins M *et al*. (2010) The impact of global warming on the tropical Pacific Ocean and El Niño. *Nat Geo* 3: 391-397.
26. Nott J, Haig J, Neil H, Gillieson D (2007) Greater frequency variability of landfalling tropical cyclones at centennial compared to seasonal and decadal scales. *Earth Plan Sci Lett* 355: 367-372.
27. Nott J (2011) A 6000 year tropical cyclone record from Western Australia. *Quat Sci Rev* 30: 713-722.
28. Toomey M, Donnelly J, Woodruff J (2013) Reconstructing mid-late Holocene cyclone variability in the Central Pacific using sedimentary records from Tahaa, French Polynesia. *Quat Sci Rev* 77: 181-189.
29. Haig J, Nott J, Reichart G-J (2014) Australian tropical cyclone activity lower than at any time over the past 550-1,500 years. *Nature* 505: 667-671.
30. Woodruff J, Donnelly J, Okuso, A (2009) Exploring typhoon variability over the mid-to-late Holocene: evidence of extreme coastal flooding from Kamikoshiki, Japan. *Quat Sci Rev* 28: 1774-1785.
31. Frappier A *et al*. (2014) Two millennia of tropical cyclone-induced mud layers in a northern Yucatán stalagmite reveal: Multiple overlapping climatic hazards during the Maya Terminal Classic "megadroughts," Geophys Res Lett 41: 5148–5157l doi:10.1002/2014GL059882.
32. Suppiah R (1992) The Australian summer monsoon: a review. *Prog Phys Geog* 16: 263-318.
33. Wheeler M, McBride, J (2011) Australasian monsoon. In: W.K.M. Lau and D.E. Waliser (eds), Intraseasonal Variability in the Atmosphere-Ocean Climate System (2nd edition). Springer, pg. 147-198.
34. Taschetto A, England M (2009) An analysis of late twentieth century trends in Australian rainfall. *Int J Clim* 29: 791-807.
35. Risbey J, Pook M, McIntosh P, Wheeler M, Hendon H (2009) On the Remote Drivers of Rainfall Variability in Australia. *Mon Wea Rev* 137: 3233–3253.
36. McGowan H, Marx S, Moss P, Hammond A (2012) Evidence of ENSO mega-drought triggered collapse of prehistory Aboriginal society in northwest Australia. *Geophys Res Lett* 39: L22702.

37. McBride J, Nicholls N (1983) Seasonal relationships between Australian rainfall and the Southern Oscillation. *Mon Weath Rev* 111: 1998-2004.
38. Taschetto A *et al*. (2010) Australian monsoon variability driven by a Gill-Matsuno type response to central-west Pacific warming. *J Clim*: 23, 4717-4736.
39. Villarini G *et al*. (2014) Sensitivity of tropical cyclone rainfall to idealized global scale forcings, *J Clim* 27: 4622-4641.
40. Lachniet M (2009) Climatic and environmental controls on speleothem oxygen isotope values. *Quat Sci Rev* 28: 412-432.
41. Lawrence J, Gedzelman S (1996) Low stable isotope ratios of tropical cyclone rains. *Geo Res Lett* 23: 527-530.
42. Frappier A, Sahagian D, Carpenter S, González L, Frappier B (2007) Stalagmite stable isotope record of recent tropical cyclone events. *Geology* 35: 111-114.
43. Klotzbach P (2011) El Niño-Southern Oscillation's impact on Atlantic basin hurricanes and U.S. landfalls. *J Clim* 24: 1252-1263.
44. Makou M, Eglinton T, Oppo D, Hughen K (2010) Postglacial changes in El Niño and La Niña behavior. *Geology* 38: 43-46.
45. Cobb K, Charles C, Cheng H, Edwards R (2003) El Niño/Southern Oscillation and tropical Pacific climate during the last millennium. Nature 424: 271-276.
46. Conroy, J.L., Overpeck, J.T., and Cole, J.E. (2010) El Niño/Southern Oscillation and changes in the zonal gradient of tropical Pacific sea surface temperature over the last 1.2 ka. *PAGES News* 18: 32-34.
47. Mann, M.E. *et al*. (2009) Global signatures and dynamical origins of the Little Ice Age and Medieval Climate Anomaly. *Science* 326: 1256-1259.
48. Khider D, Stott L, Emile-Geay J, Thunell R, Hammond D (2011) Assessing El Niño Southern Oscillation variability during the past millennium. *Paleocean* 26, PA3222.
49. Seager R *et al*. (2008) Tropical Pacific forcing of North American Medieval megadroughts: testing the concept with an atmospheric model forced by coral-reconstructed SST. *J Clim* 21: 6175-6190 .
50. Moy C, Seltzer G, Rodbell D, Anderson D (2002) Variability of El Niño/Southern Oscillation activity at millennial timescales during the Holocene epoch. *Nature* 420: 162-165.
51. Yan H, Sun L, Wang Y, Huang W, Qiu S, Yang C (2011) A record of the Southern Oscillation

index for the past 2,000 years from precipitation proxies. *Nat Geo* 4: 611-614.
52. Newton A, Thunell R, Stott L (2011) Changes in the Indonesian Throughflow during the past 2000 yr. *Geology* 39: 63-66.
53. Hall J, Matthews A, Karoly D (2001) The Modulation of tropical cyclone activity in the Australian region by the Madden–Julian Oscillation. *Mon Weath Rev* 129: 2970–2982.
54. Klotzbach P (2010) On the Madden-Julian-Atlantic hurricane relationship. *J Clim* 23: 282-293.
55. Goodwin I *et al*. (2014) A reconstruction of extratropical Indo-Pacific sea-level pressure patterns during the Medieval Climate Anomaly. *Clim Dyn* 43: 1197-1219.
56. Telcik N, Pattiaratchi C (2014) Influence of Northwest cloudbands on Southwest Australian rainfall. *J Climatol*: http://dx.doi.org/10.1155/2014/671394.
57. Frappier A (2013) Masking of inter-annual climate proxy signals by residual tropical cyclone rainwater: Evidence and challenges for low- latitude speleothem paleoclimatology. *Geochem Geophys Geosys* 14: 3632–3647; doi:10.1002/ggge.20218.
58. Mickler P *et al*. (2004) Stable isotope variations in modern tropical speleothems: Evaluating equilibrium vs. kinetic isotope effects. *Geochim Cosmochim Acta* 68: 4381-4393.
59. Knutson T *et al*. (2010) Tropical cyclones and climate change. *Nat Geo* 3: 157-163.
60. Cheng, H. *et al*. (2013) Improvements in ^{230}Th dating, ^{230}Th and ^{234}U half-life values, and U-Th isotopic measurements by multi-collector inductively coupled plasma mass spectrometry. *Earth Plan Sci Lett* 371-372: 82-91.
61. Meyers G, McIntosh P, Pigot L, Pook M (2007) The years of El Niño, La Niña, and interactions with the tropical Indian Ocean. *J Clim* 20: 2872-2880.
62. Ummenhofer C.C. *et al*. (2009) What causes Southeast Australia's worst droughts? *Geophys Res Lett* 36: L04706, doi:10.1029/2008GL036801.

Figure Legends

Figure 1. ENSO control of TC activity in the Australian region. *Top*: TC tracks (black lines) for the strong El Niño of 1982/83. Colored contours represent a composite of Aug-Dec SST anomalies for all years classified as El Niño during the period 1900-2006; SST anomalies derived using the classification by ref. 61 that was updated in ref. 62. Yellow circle defines 600 km radius from KNI-

51; CG = Chillagoe; CR = Cape Range (ref. 29). TC track data were obtained from www.ncdc.noaa.gov/ibtracs/index.php?name=ibtracs-data. *Bottom*: same as top except TC tracks are for the strong La Niña of 1988/89 and colored contours represent Aug-Dec SST anomalies for all years classified as La Niña.

Figure 2. Flood markers in cave KNI-51. *Left:* Photograph of slabbed interior of stalagmite KNI-51-11 showing ages and errors of dated intervals (in year CE) and flood layers (black arrows); note preferential preservation of sediment on margins of growth surfaces, likely as a result of erosion of sediment by dripwater striking center of stalagmite cap after floodwaters had receded. Orange rectangles denote positions of dated intervals. *Right:* Flood staining in KNI-51 associated predominantly with extreme rainfall events derived from TCs; white arrows denote peak flood level.

Figure 3. Role of TCs in extreme rainfall events. Peak annual consecutive 1-, 2-, and 3- day rainfall totals for Carlton Hill Station for the period of calibration (x-axis in years CE). Gaps represent periods of incomplete data collection at the station. Blue and grey circles denote rainfall derived from TCs within a 600 km radius of KNI-51, while white circles denote rainfall associated with events not assigned to TCs. Dashed lines denote the rainfall thresholds exceeded only by TCs (blue circles). TC rainfall varies greatly, and depends on storm intensity, distance from the weather station, and duration and track through the area. Thresholds are 150 mm for 1-day, 200 mm for 2-day, and 250 mm for 3-day consecutive events.

Figure 4. Comparison of Australian, Atlantic, and Caribbean TC reconstructions and ENSO proxies. A: Flood occurrences (30-yr running mean) preserved in KNI-51 stalagmites (each denoted by a different color). Dashed lines represent multi-centennial averages. B-D: hurricane reconstructions from (B) Florida (red) (14); (C) Belize (green) (15); (D) Puerto Rico (blue) (18); hurricane activity is related to mean grain sizes of sediments which, for ease of presentation, are plotted on a log-scale; and ENSO reconstructions (E) La Niña events (orange) (44); elevated cholesterol values indicate increased frequencies of La Niña events; in order to maintain consistent temporal resolution throughout the time series, the youngest two data points represent an average of multiple, more closely spaced analyses; and (F) Indonesian Throughflow values reconstructed using Makassar Straight south - north seawater density differences assessed with foraminifera oxygen isotopic ratios (purple) (52); higher (less negative) values represent more La Niña-like conditions. Blue shaded regions denote periods of elevated flood occurrences at the KNI-51. For ease of presentation, in B-F, y-axis truncates 1890 CE peak in KNI-51-11 flood occurrences.

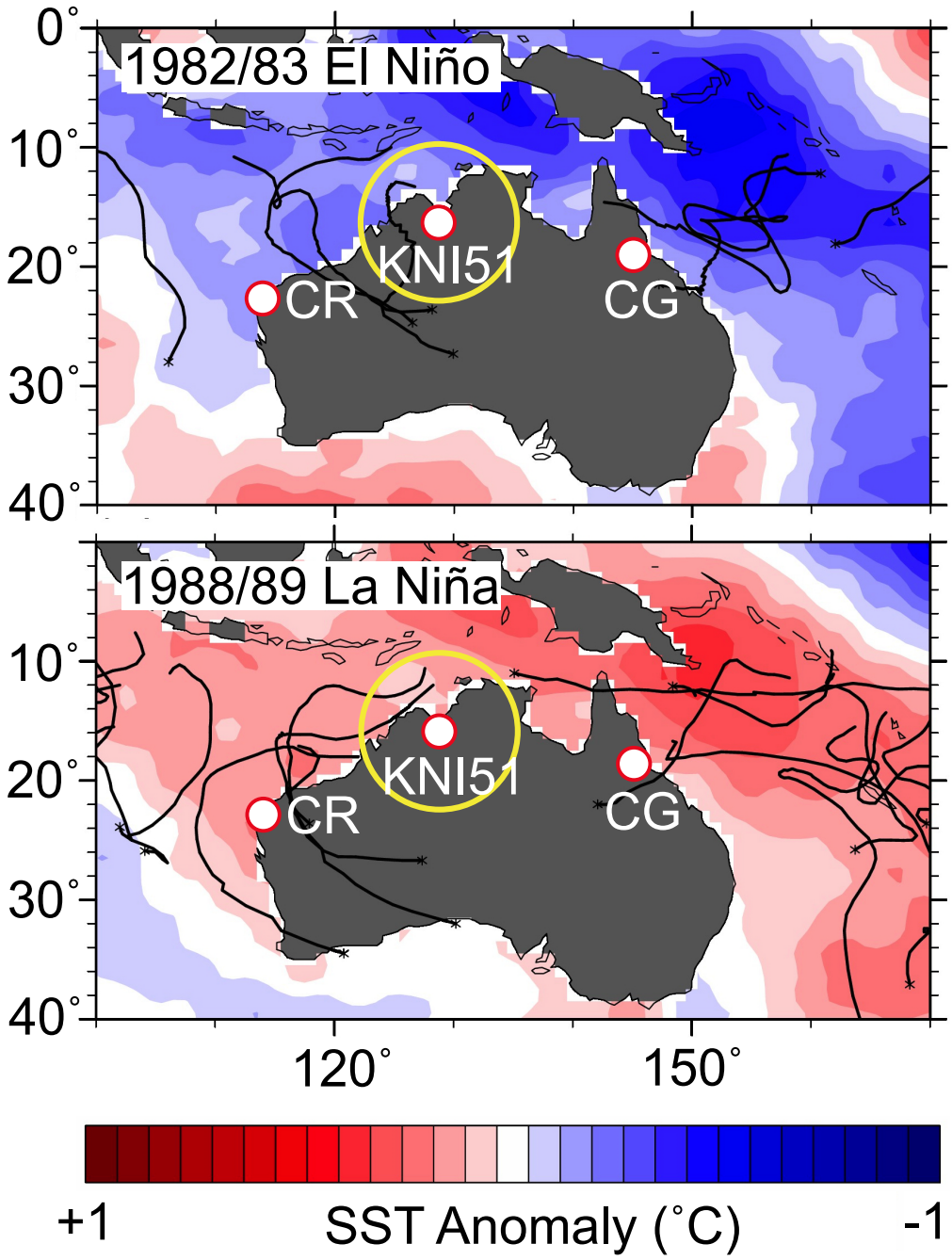
1982/83 El Niño
KNI51
CR
CG
1988/89 La Niña
KNI51
CR
CG
0°
10°
20°
30°
40°
120°
150°
+1
SST Anomaly (˚C)
-1

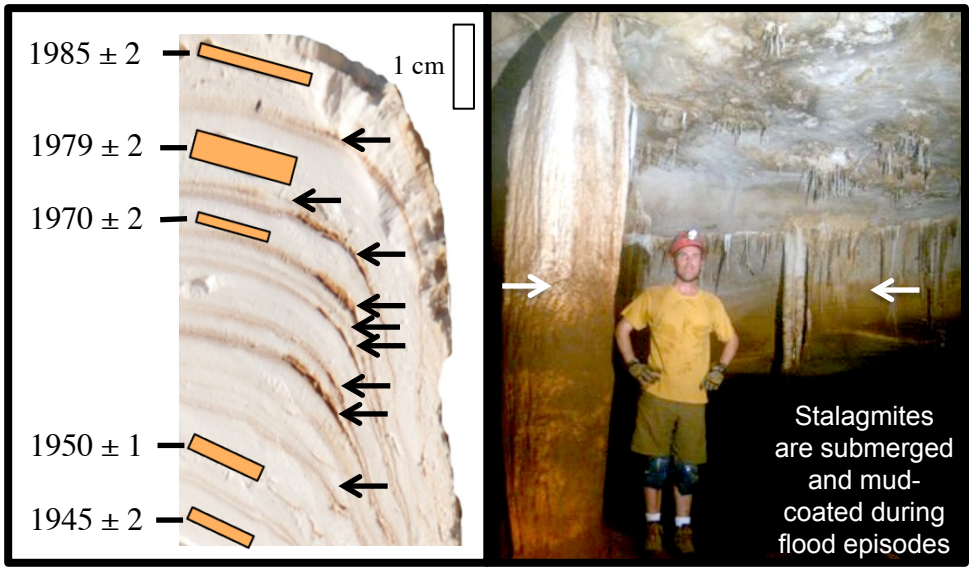
1985 ± 2
1979 ± 2
1970 ± 2
1950 ± 1
1945 ± 2
1 cm
Stalagmites are submerged and mud-coated during flood episodes

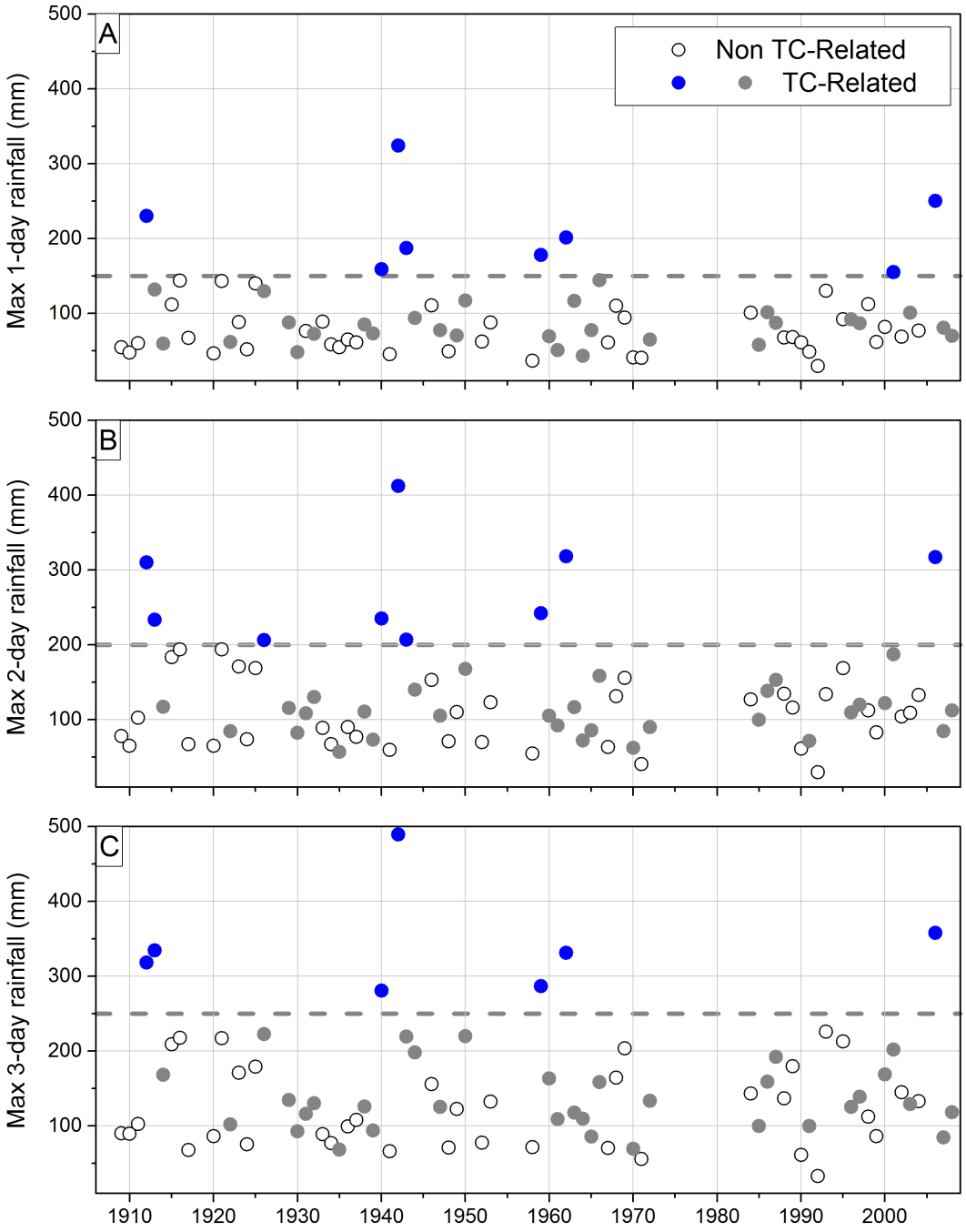
A
B
C
Non TC-Related
TC-Related
Max 1-day rainfall (mm)
Max 2-day rainfall (mm)
Max 3-day rainfall (mm)
100
200
300
400
500
1910
1920
1930
1940
1950
1960
1970
1980
1990
2000

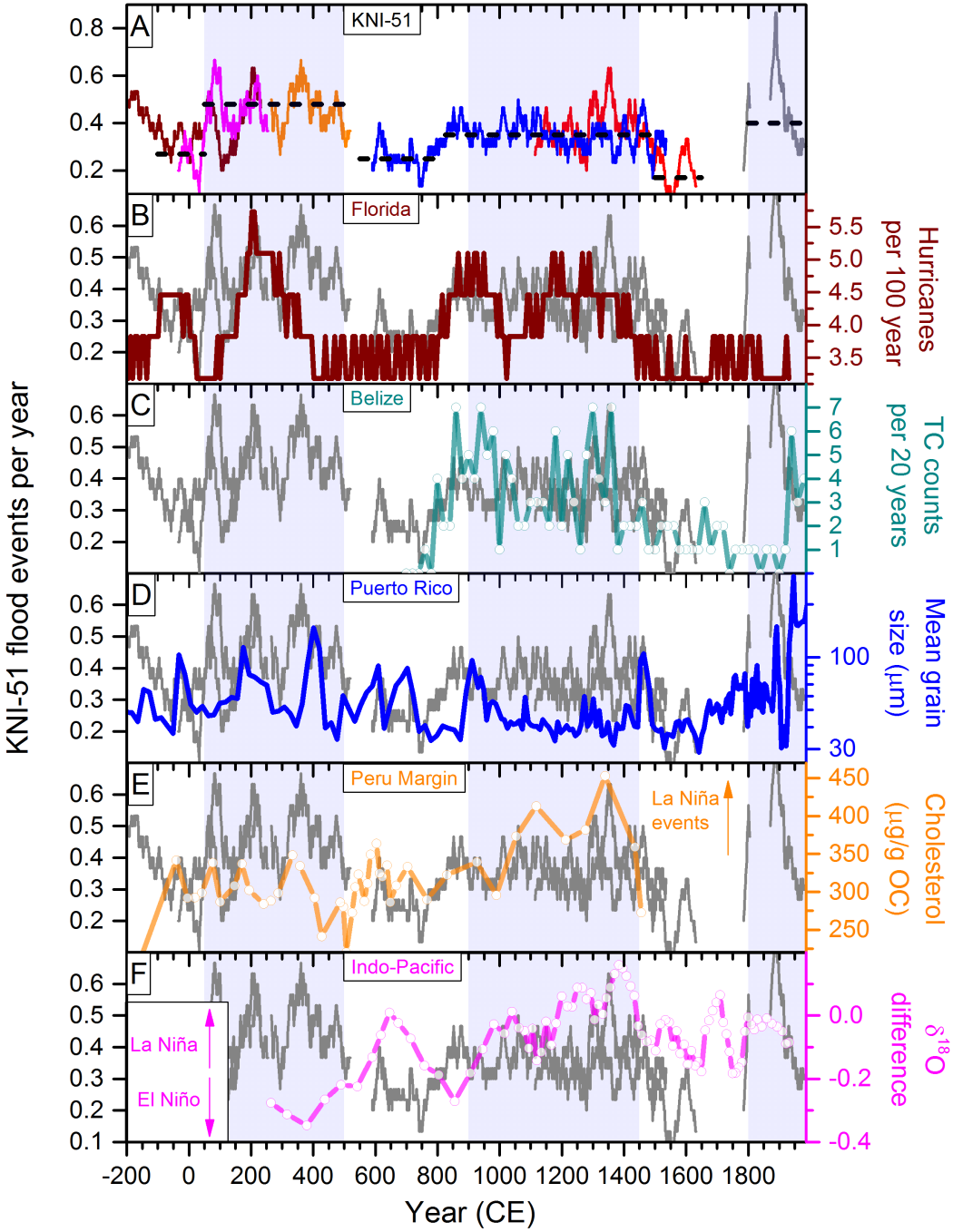
A
KNI-51
B
Florida
Hurricanes per 100 year
C
Belize
TC counts per 20 years
D
Puerto Rico
Mean grain size (μm)
E
Peru Margin
La Niña events
Cholesterol (μg/g OC)
F
Indo-Pacific
La Niña
El Niño
δ18O difference
KNI-51 flood events per year
Year (CE)

SI Appendix

Preservation/Identification of Flood-Deposited Sediment on Stalagmite Surfaces. In addition to those discussed in the text, several factors influence our ability to link TCs to cave flooding:

Distance vs Intensity Relationships - Large storms distal to the cave may produce rainfall events commensurate with more proximal but smaller storms. Studies of South Pacific TCs found a pronounced decrease in rainfall with distance, particularly after 600-700 km from the eye of the storm (1). Thus, in order to test the 600 km radius window we used to develop our calibration, we also calculated the peak annual single and multi-day rainfall totals for TCs within 500 km (Fig. S7). The differences in results between the 500- and 600-km buffers are minor, with most of the offset for low rainfall values; all the large events are still associated with TCs.

Closely Occurring TCs - TCs routinely occur in close succession within a single season. For example, TC Fay and TC Evan both passed within 400 km of KNI-51 during March 2004, and TC Debbie reached a similar distance in December 2003. Because flooding of the cave is required to deposit mud on stalagmite caps, and because stalagmite growth may not occur immediately after floodwaters recede, multiple TCs within the same season may not be individually recorded or be distinguishable from one another.

TC Track and Speed – Rainfall intensity at a site is a function of the residence time of a storm and the path the storm has followed to that site. TCs weaken rapidly over land and thus wind speeds and rainfall amounts typically decrease markedly after landfall (2). However, circular storm tracks may increase the time a storm impacts a given site and thereby increases rainfall totals there. For example, in February 2011, TC Carlos made landfall near Darwin and doubled back on the area, dropping 684 mm of rain in the process. However, its subsequent track took it inland to the west where rainfall of only 90 mm was recorded at Wyndham several days

later. In 1986, within error of the largest mud layer in KNI-51-11, TC Hector made landfall just northeast of KNI-51, resulting in intense rainfall that caused 200-year flooding on the Fitzroy River and the evacuation of hundreds of people from nearby Wyndham. Rainfall associated with this event reached the 90th percentile for all Januaries on record (from 1898) at Carlton Hill Station. In addition, TC Carlos tracked close to KNI-51 in February 2011, dropping 90 mm of rain; TC Lua made landfall in western Kimberley in 2012, with three-day rainfall of >500 mm.

Storage Effects – Cave flooding should reflect not only the rainfall associated with a particular storm event but also the available water storage space in the watershed and in the bedrock overlying the cave. Thus, long-term area and cave-specific monitoring is required to formally define the exact nature of the cave flood threshold. However, drips had ceased in KNI-51 when visited in June 2009 and June 2011, approximately 1-2 months after the end of the monsoon season, suggesting limited storage capacity above this cave.

Changes in Growth Direction – The thickest mud layers in stalagmite KNI-51-11 are associated with a change in growth direction, suggesting that the stalagmite shifted its position on its mud substrate during large flood events. Such a change in geometry complicates age-distance relationships between radiometric dates and can interfere with the preservation of mud on the stalagmite cap. This problem is limited here due to the high density of high-precision dates. Growth direction changed several times during its history, each time in association with a thick layer of sediment (Type 3 layer).

Diagenetic Alteration – Isolated areas in sample KNI-51-O are recrystallized from finely crystalline primary aragonite to more coarsely crystalline calcite. Where such alteration has occurred, the change in crystal fabric obscures mud layers, making their identification/ classification slightly more difficult. In this case, however, affected portions are on a cm-scale

near the central growth axis and in no cases were entire growth bands fully obscured. Thus, mud layers were easily discernable, and these areas were avoided for dating. Relatedly, no dissolution or alteration is apparent on any growth surfaces (bounding layers) immediately below mud layers as would have occurred if dripwater had become corrosive prior to cave flooding (3).

Modern environmental setting. Onset of IASM rainfall in the Kimberley typically occurs in mid- to late December, with the poleward displacement of the subtropical jet and ridge. Tropical cyclone genesis regularly occurs in association with the monsoon trough which separates trade wind easterlies on its southern side from westerly winds between the monsoon trough and the equator, and slopes towards the equator with increasing height (4). The position of the monsoon shear line over northwestern Australia relates to the Pilbara Heat Low, reflecting landmass diabatic forcing and limiting the poleward extent of the summer monsoon regime. The monsoon trough extends well north of the continent with maximum cloudiness located at 0 to 5ºS and 5˚ to 10ºS. Over the region of the Maritime Continent the high SSTs provide a broad, ill-defined area of strong convection, indicated by the outgoing longwave radiation (OLR) pattern over the region, which can be strikingly different from the well-defined structure and latitudinal position of the OLR patterns associated with the intertropical convergence zone over the adjacent Pacific and Indian oceans (5). The onset corresponds to a dramatic increase in zonal winds over an approximately 90˚ longitude region. The strong convection that is contained within the westerly flow, extends over a large region, and locates monsoon depressions.

Possible effects of humans on surface hydrology and the KNI-51 flood record. There can be no doubt that the ecosystems of the Australian tropics have been strongly influenced by human

activity, starting with burning by Aboriginal peoples in the late Pleistocene (6) and including pastoral and agricultural practices by descendants of European settlers beginning in the 19th century. Cattle grazing in the eastern Kimberley, including at Carlton Hill Station, began in the late 19th century (7). The denudation of some plant species, coupled with soil compaction and other effects associated with the introduction of cattle has been shown to increase run-off and soil erosion rates (8-9), and thus we interpret the large spike in cave flooding events in the 1890s likely as reflective of changes in land-use practices. If so, then the sensitivity of cave flooding to rainfall during the calibration period (1906-1986 CE) may have been somewhat greater relative to the earlier portions of the stalagmite record. However, it is unclear what impact these changes had on our rainfall/flood event calibration, and this does not change the underlying facts that TCs contribute the majority of extreme rainfall events and that the highest rainfall totals are logically the most likely to be associated with flooding. Similarly, it is worthwhile considering the susceptibility of the full range of our flood layer time series (the last 2200 years) to prehistoric landscape changes, but little independent evidence exists for substantive human-induced changes to vegetation type over this time (10-12).

References

1 - Villarini, G. *et al*. (2014) Sensitivity of tropical cyclone rainfall to idealized global scale forcings. *J Clim* 27: 4622-4641.

2 - Vickery P, Masters F, Powell M, Wadhera D (2009) Hurricane hazard modeling: The past, present, and future. *Jour Wind Eng Ind Aero* 97: 392 – 405.

3 – Railsback L, Akers P, Wang L, Holdridge G, Voarintsoa N (2013) Layer-bounding surfaces in stalagmites as keys to better paleoclimatological histories and chronologies. Int J Speleo

42: 167–180.

4 - McBride J (1987) The Australian summer monsoon. In: C. P. Chang and T. N. Krishnamurti (eds), Monsoon Meteorology. Oxford University Press, New York, 203–231.

5 - Walliser D, Gautier C (1993) A satellite-derived climatology of the ITCZ. *J Clim* 6: 2162-2174.

6 - Miller G, Magee J, Fogel M, and Gagan M (2007) Detecting human impact on the flora, fauna and summer monsoon of Pleistocene Australia. *Clim Past* 3: 463–473.

7 - Durack (1972) Australian Dictionary of Biography; http://adb.anu.edu.au/biography/durack-patrick-3457.

8 - Bartley, R. *et al*. (2006) Runoff and erosion from Australia's tropical semi-arid rangelands: influence of ground cover for differing spaces and time scales. *Hydrol Proc* 20: 3317-3333.

9 - Carroll, C. *et al*. Sediment erosion research in the Fitzroy basin central Queensland: an overview. 19th World Congress of Soil Science, Soil Solutions for a Changing World 167 1 – 6 August 2010, Brisbane, Australia (2010).

10 - McGowan H, Marx S, Moss P, Hammond A (2012) Evidence of ENSO mega-drought triggered collapse of prehistory Aboriginal society in northwest Australia. *Geophys Res Lett* 39: L22702.

11 - van der Kaars S, De Deckker P, Gingel F (2006) A 100 000-year record of annual and seasonal rainfall and temperature for northwestern Australia based on a pollen record obtained offshore. *J Quat Sci* 21: 879-889.

12 - Denniston R *et al*. (2013) A Stalagmite Record of Holocene Indonesian-Australian Summer Monsoon Variability from the Australian Tropics. *Quat Sci Rev* 78: 155-168; 10.1016/j.quascirev.2013.08.004.

Fig. S1. KNI-51 stalagmites discussed in this study. For ease of presentation, scales of individual samples were adjusted individually but cm demarcations are visible along central growth axes.

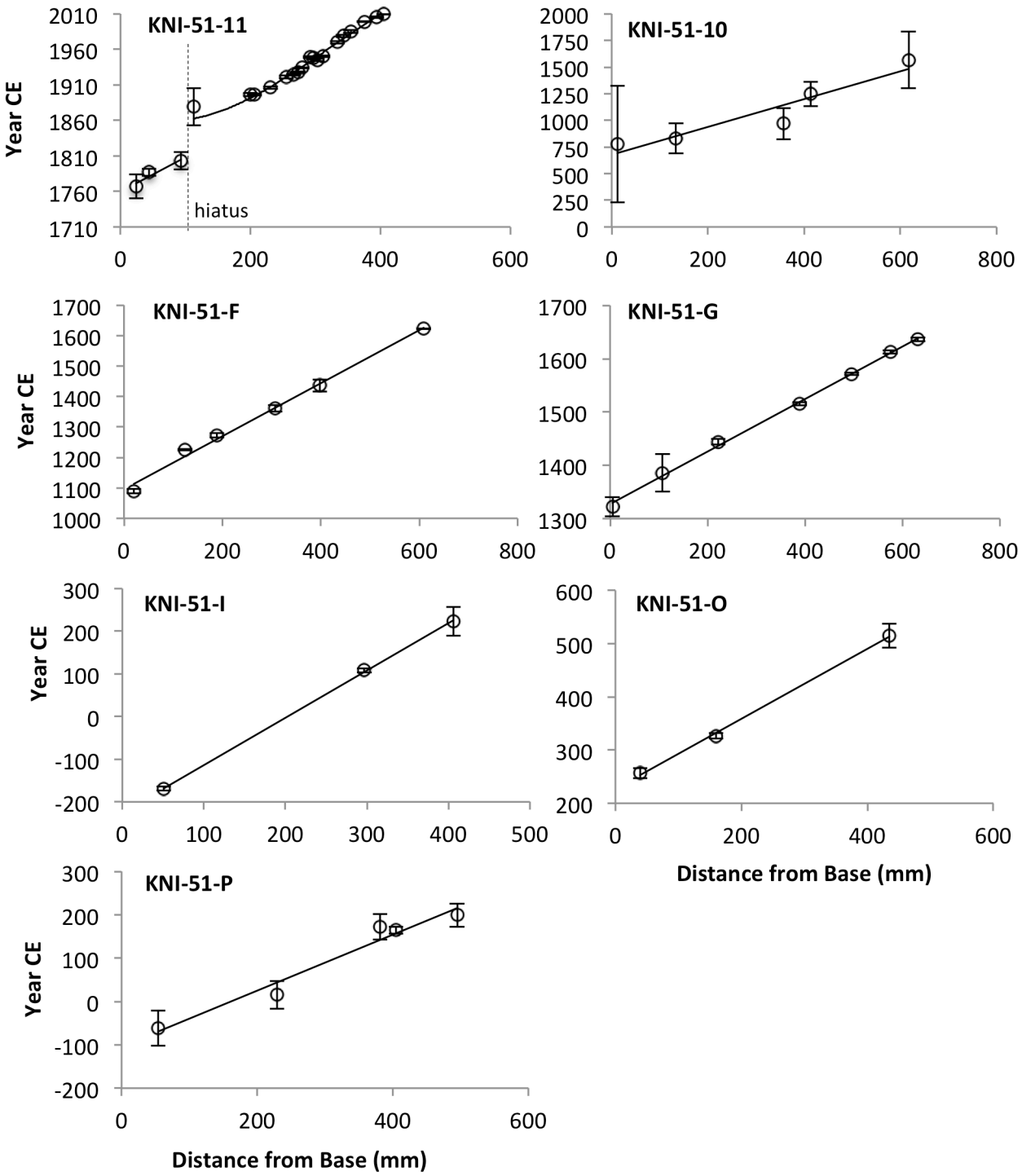

Fig. S2. ^{230}Th dates and age models. Vertical lines represent 2 standard deviation errors. Dates for all stalagmites other than KNI-51-11 are from ref. 11.

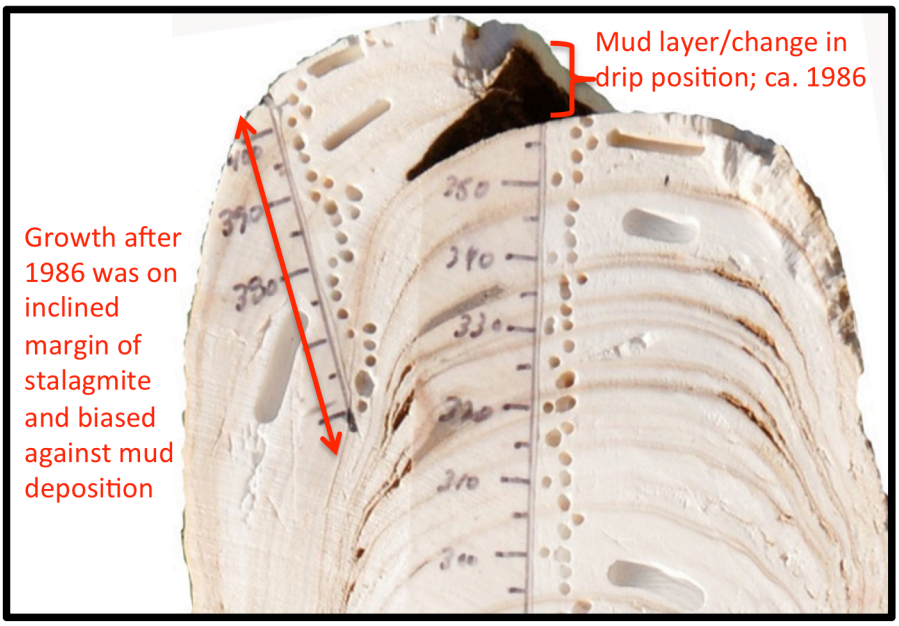

Fig. S3. Top of stalagmite KNI-51-11 showing change in growth position after ~1986 CE that resulted in an inclined margin that appears to have limited preservation of flood-derived sediment. Given its geometry, it is likely that following retreat of cave floodwaters, re-establishment of drips onto the active growth surface were highly effective at eroding any flood-derived sediment. A more horizontal growth surface did not re-develop until approximately 2008.

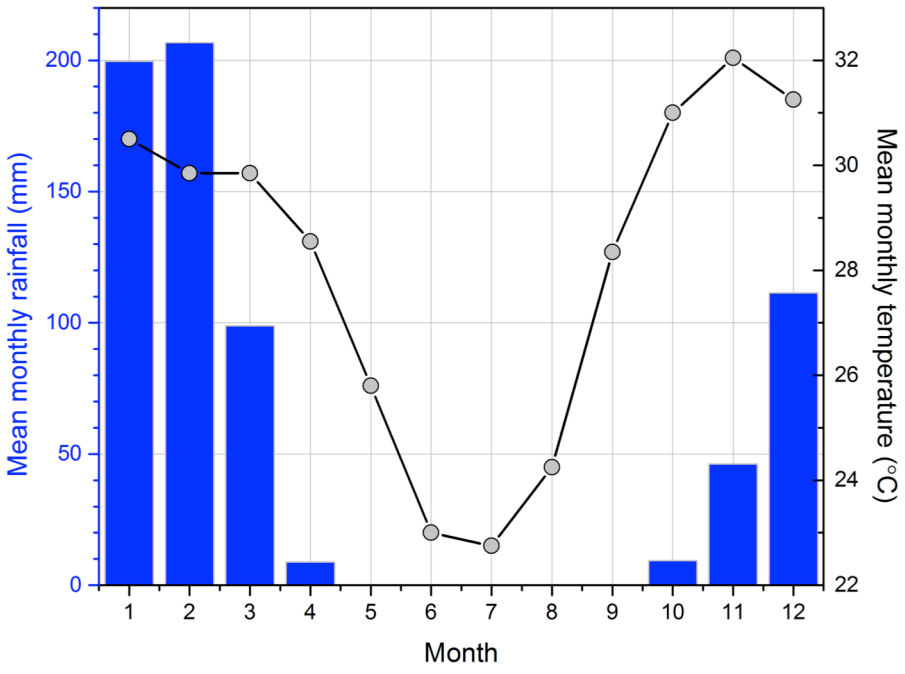

Fig. S4. Monthly rainfall (blue bars) and temperature (grey circles) values from the town of Kununurra, Western Australia, located approximately 50 km from KNI-51 (www.bom.gov.au).

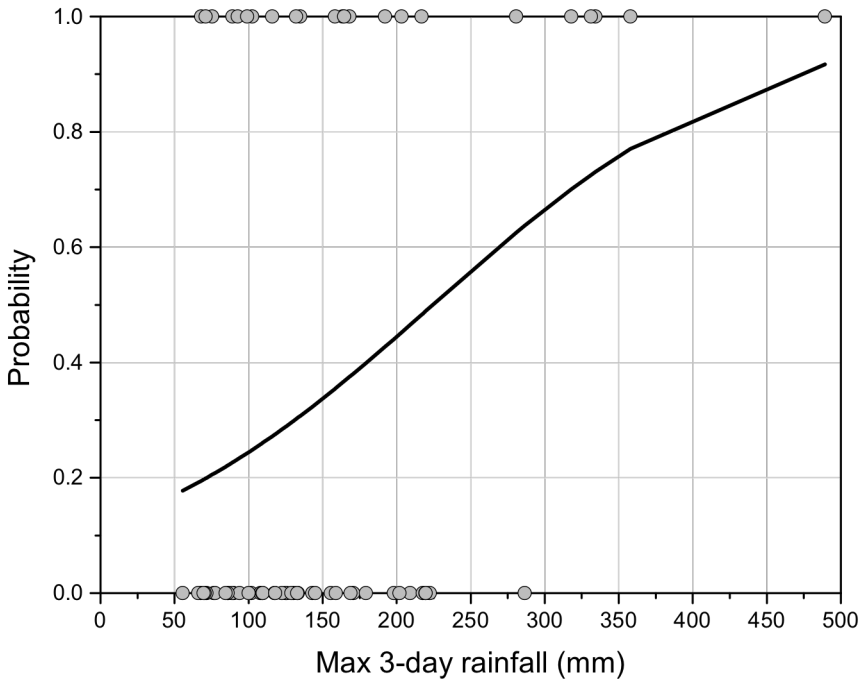

Fig. S5. Logistic model of rainfall thresholds for cave flooding events. The values "1" and "0" represent the occurrence and non-occurrence of a flood event, respectively, for different values of maximum three-day rainfall. The black line represents the fitted logistic model; p-value<0.015.

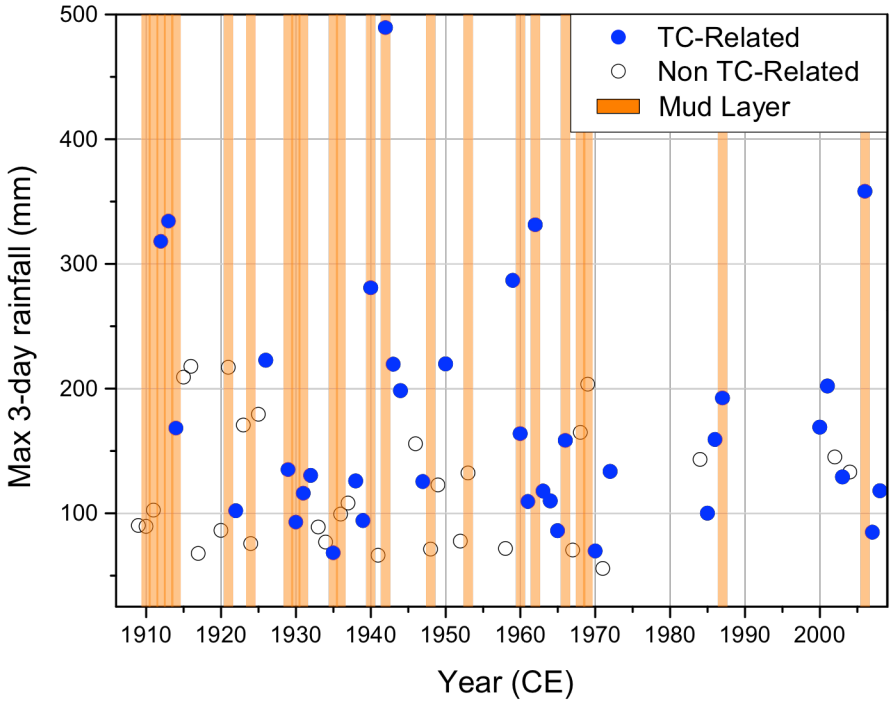

Fig. S6. Three-day peak annual rainfall totals (blue circles for events tied to TCs and white circles for events tied to non-TC rainfall) for Carlton Hill Station with correlations to flood layers (vertical orange bars) from stalagmite KNI-51-11. Ages of the flood layers have been shifted by up to ±1 yr (minimum age uncertainties from ^{230}Th dates) to determine a maximized correlation with three-day peak rainfall events. In doing so, the ages of all mud layers were shifted uniformly, the most conservative possible tuning method, rather than individually which would have yielded a higher correlation. Gaps in the record represent periods of incomplete rainfall data collection. In most cases, the highest rainfall totals are associated with TCs and can be temporally aligned with stalagmite flood events.

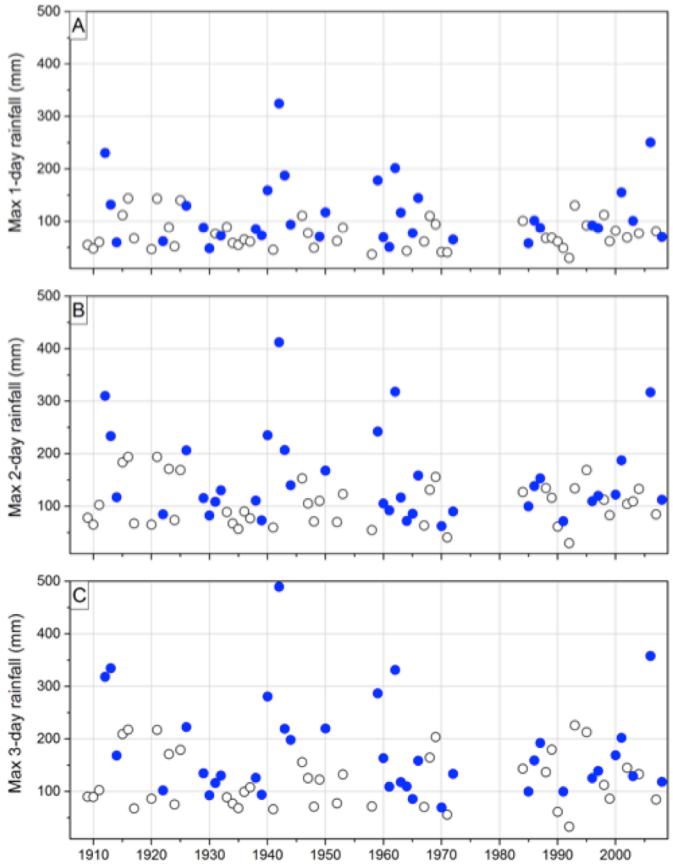

Fig. S7. From A-C: Peak annual consecutive 1-, 2-, and 3- day rainfall totals for Carlton Hill Station for the period of calibration (x-axis in years CE) using a 500 km radius window. Gaps represent periods of incomplete data collection at the station. Blue circles denote rainfall derived from TCs within 500 km radius of KNI-51, while open circles denote rainfall associated with events not assigned to TCs.

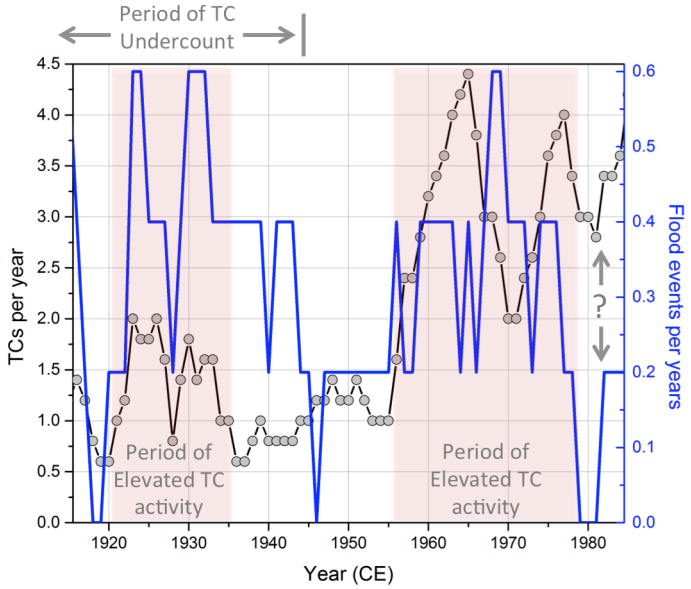

Fig. S8. Five-year running means of observed TC events within 600 km of cave KNI-51 for the period 1908-1986 CE (black line) with flood events from stalagmite KNI-51-11 (blue line). The accuracy of the TC count likely declines prior to the start of the satellite era (1970 CE) and this undercount is particularly evident in the interval of peak TC activity from 1920-1935. Increases in TC activity are recorded for the same intervals (pink shaded areas) in both the historical and stalagmite records. TC track data were obtained from www.ncdc.noaa.gov/ibtracs/index.php?name=ibtracs-data.

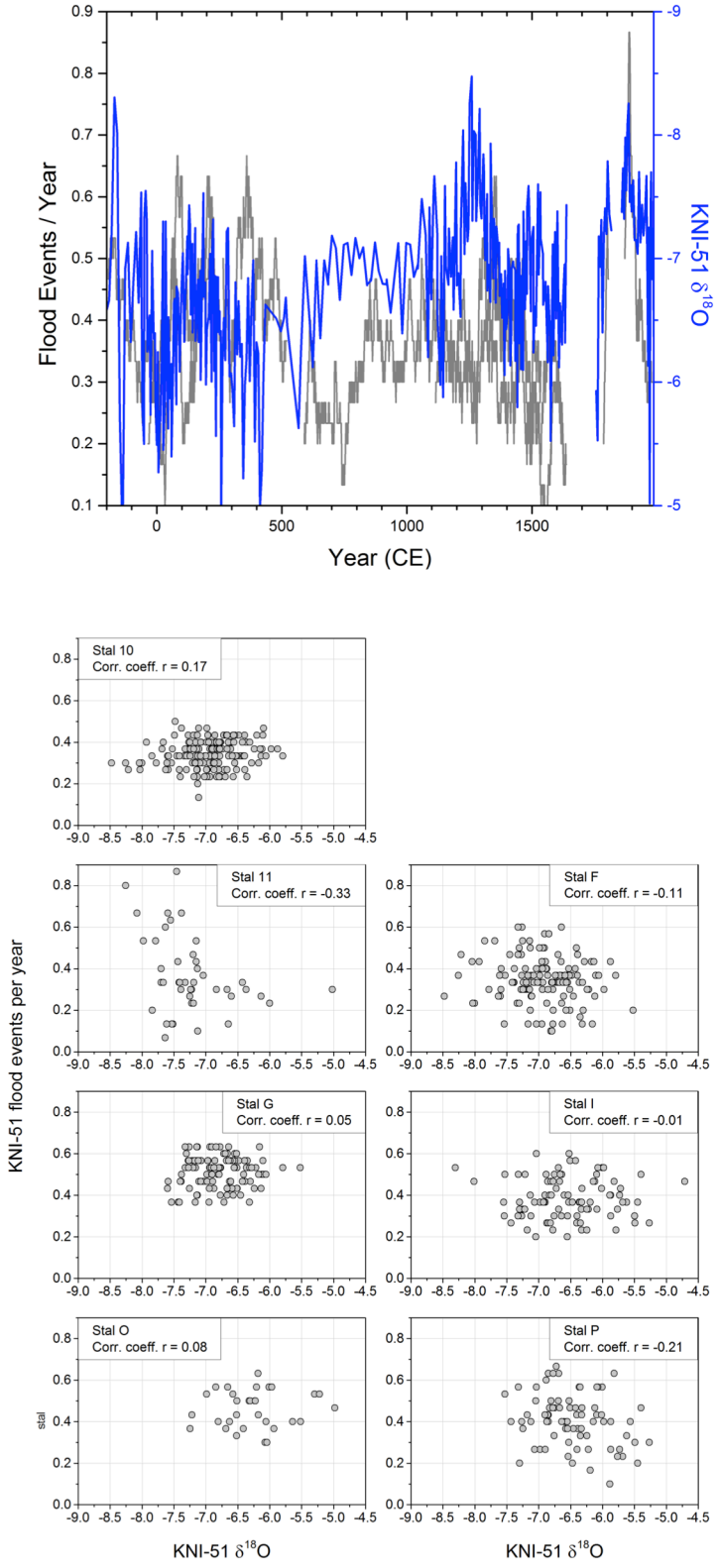

Fig. S9. Top: Flood layer and IASM variability. Comparison of KNI-51 flood record (grey line) with IASM reconstruction derived from oxygen isotopic values from the same stalagmites[8] (blue). Flood layer values from KNI-51-G were reduced by 0.2 to account for observed offset. Stronger IASM is up on the y-axis. Bottom: Correlation between oxygen isotopic ratios and flood events from individual KNI-51 stalagmites. A negative correlation would result from a strengthened monsoon which would increase the likelihood of cave flooding while simultaneously enhancing amount effect-related ^{18}O depletion in rainwater.

Fig. S10. Mud layer types (T). Majority of the sediment associated with the Type 3 layer (right panel) has been removed. Linear trough is area milled for dating. Note that stalagmite growth surfaces associated with mud layers do not appear to suffer from corrosion, suggesting rapid submersion by floodwaters. Mud preservation is typically most evident on the margins of stalagmite growth surfaces, likely because dripwaters erode newly deposited mud from central growth axis.

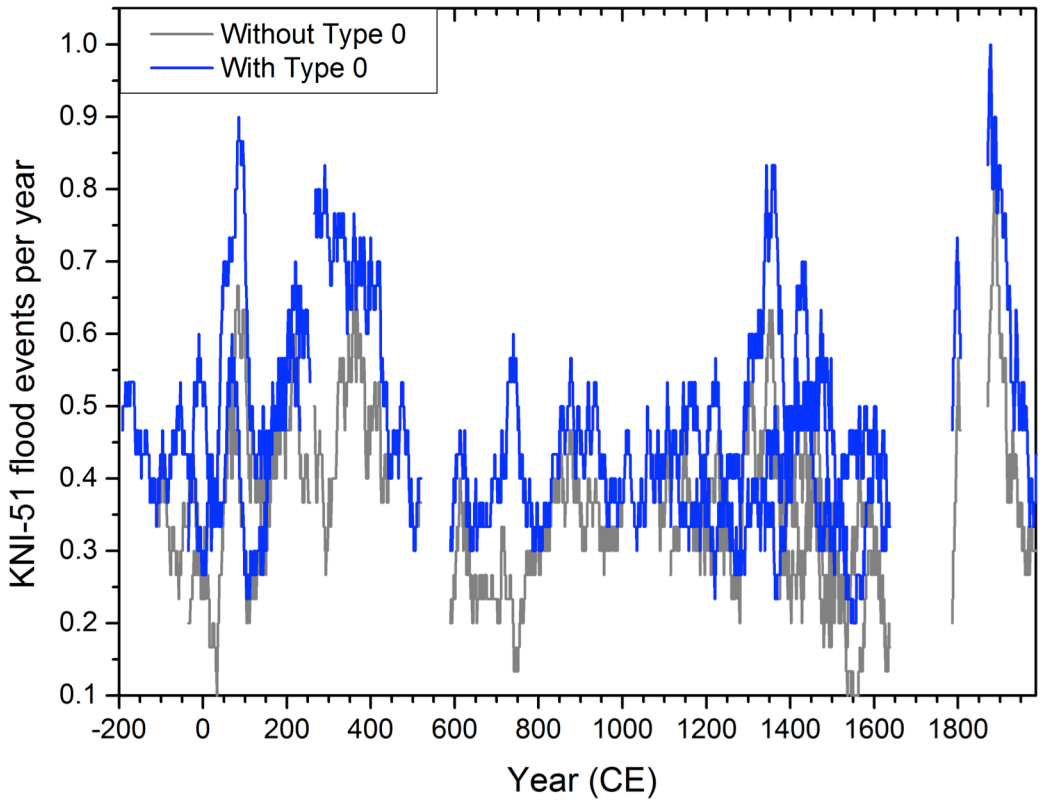

Fig. S11. Influence of Type 0 mud layers on flood layer time series. Composite flood layer time series including (grey line) and excluding (blue line) Type 0 mud layers. Type 0 flood layers were excluded from the primary flood reconstruction because their nature and origin is unclear, but may be an artifact of biases in mud layer preservation. This figure provides a qualitative test of the impact of including these layers and reveals a minimal impact on temporal trends.

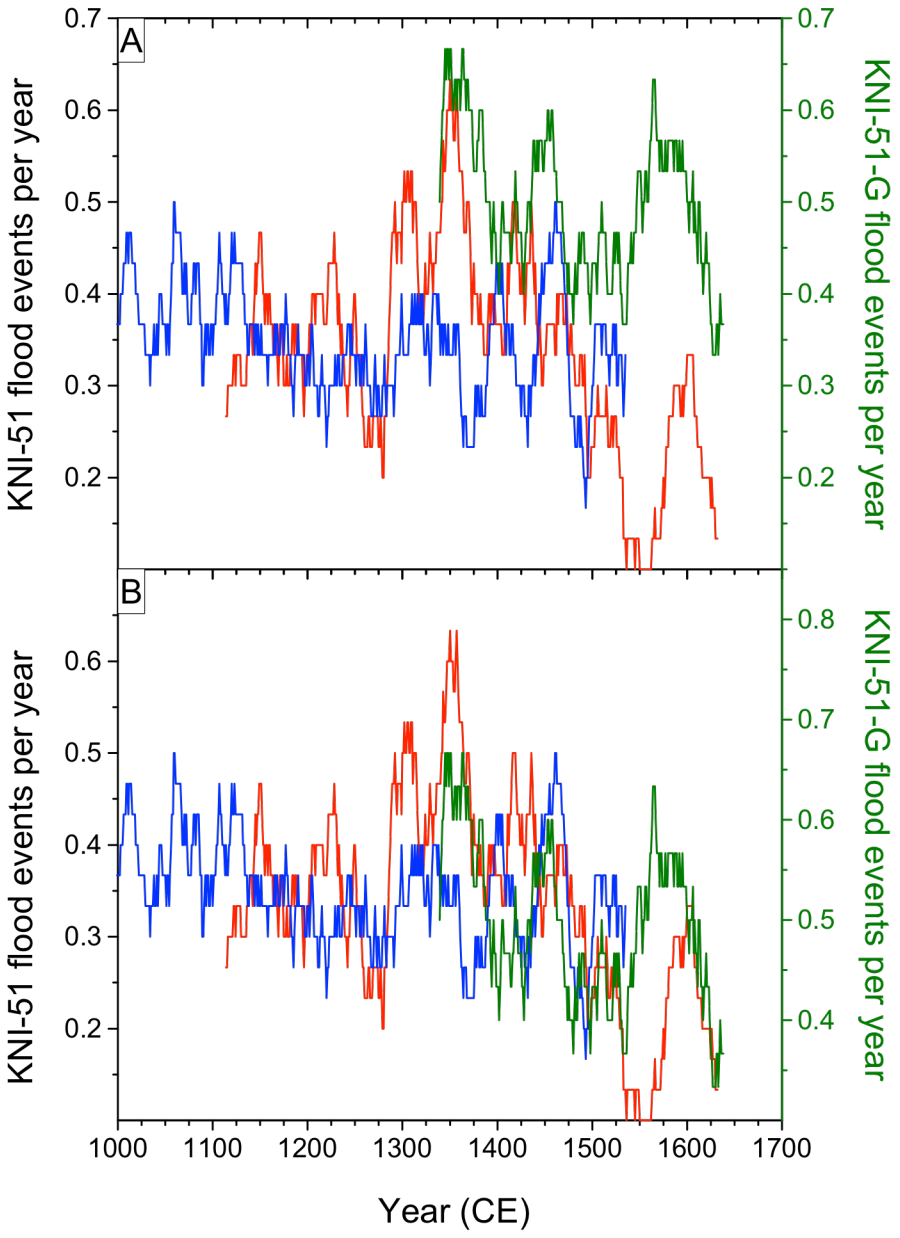

Fig. S12. Comparison of KNI-51-G (right axis) and two coeval stalagmites (left axis) with (A) same scales, and (B) right y-axis compressed to illustrate similar trends between coeval samples. The origin of the elevated numbers of flood layers recorded in stalagmite KNI-51-G is unclear, however the similar trends, both at multi-decadal and multi-centennial scales, suggests that trends in flooding frequency is consistently recorded by each sample.

SI Table 1

Sample	Distance to Base (mm)	^{238}U (ng/g)	^{232}Th (pg/g)	$\delta^{234}U$[a] (corr'd)	Error[b]	$^{230}Th/^{238}U$ (activity)	Error	$^{230}Th/^{232}Th$ (ppm)	Error	Uncorrected Age (yr)	Error (yr)	Corrected Age (yr CE)[c]	Error (yr)
11[d]	405	10,238	1,488	1,338.4	1.1	0.00003	0.00001	3.8	1.5	2	1	2010	1
11	394	5,281	3,046	1,339.0	1.8	0.00009	0.00003	2.5	0.8	4	1	2005	1
11	375	7,458	774	1,341.4	1.6	0.00024	0.00001	38.8	2.0	11	1	1999	1
11	354	5,191	1,382	1,353.5	1.1	0.00058	0.00003	36.3	2.1	27	1	1985	2
11	343	8,557	2,129	1,365.3	1.1	0.00072	0.00001	47.9	1.0	33	1	1979	2
11	334	6,537	2,241	1,366.7	2.4	0.00100	0.00001	48.2	0.9	46	1	1970	2
11	311	6,894	1,505	1,352.4	2.4	0.00138	0.00001	104.6	2.4	64	1	1950	1
11	303	6,311	1,483	1,374.0	2.4	0.00152	0.00002	106.7	2.9	70	1	1945	2
11[d]	297	6,049	643	1,380.3	1.0	0.00139	0.00002	215.5	11.8	64	1	1948	1
11	292	12,297	14,153	1,355.1	0.8	0.00162	0.00001	23.2	0.2	75	1	1949	7
11	280	5,484	137	1,376.3	0.8	0.00165	0.00002	1,091.3	201.8	76	1	1934	1
11	273	11,346	652	1,357.8	2.4	0.00183	0.00001	524.8	22.7	85	1	1928	1
11	266	9,866	513	1,351.3	0.8	0.00177	0.00001	560.6	33.3	82	1	1924	1
11	255	7,711	1,395	1,359.4	1.2	0.00198	0.00001	180.5	3.9	92	1	1921	1
11	231	8,105	2,580	1,345.2	2.3	0.00235	0.00002	122.0	2.3	110	1	1906	2
11[d]	206	6,382	579	1,358.8	1.9	0.00246	0.00003	446.8	32.1	114	1	1896	1
11	200	6,763	2,347	1,360.7	1.0	0.00250	0.00002	119.1	2.4	116	1	1896	2
11[d]	93	4,686	4,432	1,359.9	1.7	0.00472	0.00004	82.4	1.0	219	2	1803	12
11[d]	44	5,321	6,216	1,354.6	1.9	0.00511	0.00005	72.2	0.8	237	2	1787	5
11	24	5,189	7,090	1,323.7	1.4	0.00553	0.00005	66.9	0.7	260	2	1767	17

[a] $\delta^{234}U = [(^{234}U/^{238}U)/(^{234}U/^{238}U)_{eq}-1] \times 10^3$, where $(^{234}U/^{238}U)_{eq}$ is the secular equilibrium activity ratio; values in permil.

[b] Errors at presented at the 2 standard deviation level.

[c] An intial $^{230}Th/^{232}Th$ atomic ratio of $4.4 \times 10^{-6} \pm 50\%$ was used to correct detrital ^{230}Th. Ages also corrected for year of analysis.

[d] These dates previously published in ref. 1 using an initial Th correction of $4.4 \times 10^{-6} \pm 100\%$.